This is a preprint, the final version is subject to change, of the American Mineralogist (MSA)
Cite as Authors (Year) Title. American Mineralogist, in press.
(DOI will not work until issue is live.) DOI: http://dx.doi.org/10.2138/am-2014-4690

REVISION 3

The occurrence and composition of chevkinite-(Ce) and perrierite-(Ce) in tholeiitic intrusive rocks and lunar mare basalt

Janet R. Muhling[1,2*], Alexandra A. Suvorova[1] and Birger Rasmussen[2]

[1]Centre for Microscopy, Characterisation and Analysis, The University of Western Australia, Crawley, WA 6009, Australia

[2]Department of Applied Geology, Curtin University, Kent St, Bentley WA 6102, Australia

[*]*E-mail: janet.muhling@uwa.edu.au*

ABSTRACT

Chevkinite-(Ce) and perrierite-(Ce) are the most common members of the chevkinite group of minerals. They are dimorphs, and both have the general formula $A_4BC_2D_2Si_4O_{22}$, where A = REE, Y, Ca, Sr, Th; B = Fe^{2+}, (Mn, Mg); C = Ti, Al, Fe^{3+}, Fe^{2+}, Cr, Mn, Mg, Zr, Hf, Nb; and D = Ti. Both have been reported from a wide range of igneous, metamorphic and hydrothermal rocks types, but occurrences in mafic rocks are rare, with minimal chemical and crystallographic documentation. Chevkinite-(Ce) and/or perrierite-(Ce) occur with other Ti-, Zr- and REE-bearing accessory phases in eight suites of tholeiitic dolerite from Western Australia, and in lunar mare basalt 10047. They are more abundant than has been recognized previously in mafic igneous rocks, and are significant hosts of incompatible elements. Chevkinite-(Ce) and perrierite-(Ce) from mafic rocks have distinctive chemical compositions with higher Zr than recorded in examples from most other common rock types. Among mafic rocks, two groups are recognized based on total Fe contents in electron microprobe analyses: crystal structural

analysis by electron diffraction indicates that the high-Fe group (>8 wt% FeO) is chevkinite-(Ce) while the low-Fe group (<8 wt% FeO) is consistent with perrierite-(Ce), and both minerals can occur within a single hand specimen. A previously proposed chemical discriminant is not applicable to chevkinite-group minerals from typical mafic igneous rocks and crystal structural information is required to unequivocally distinguish between the two dimorphs.

Key words: Chevkinite, perrierite, tholeiitic dolerite, lunar mare basalt, chemical (mineral) analysis, electron diffraction

INTRODUCTION

The chevkinite group of minerals comprises common, although not abundant, accessory minerals. The most common members of the group are chevkinite-(Ce) and perrierite-(Ce). Both are Ti-Fe-REE (rare earth element) silicates with the general formula $A_4BC_2D_2Si_4O_{22}$, where A = REE, Y, Ca, Sr, Th; B = Fe^{2+}, (Mn, Mg); C = Ti, Al, Fe^{3+}, Fe^{2+}, Cr, Mn, Mg, Zr, Hf, Nb; and D = Ti (e.g., Macdonald and Belkin 2002). Trace amounts of a wide range of other elements may substitute in both minerals, but chemical analyses show that they are close to stoichiometric despite metamictization and, in some cases, hydration.

Both chevkinite-(Ce) and perrierite-(Ce) are found in a wide range of rock types (Macdonald and Belkin 2002 and references therein), including intrusive and volcanic igneous rocks (Macdonald et al. 2002; Troll et al. 2003; Jiang 2006; Vlach and Gualda 2007; Carlier and Lorand 2008; Prol-Ledesma et al. 2012; Macdonald et al. 2013), metasomatized or hydrothermal rocks such as fenites and ore deposits (Macdonald et al. 2012), and metamorphic rocks including granulite facies gneisses (Belkin et al. 2009) and metacarbonates (Macdonald et al. 2009). Chevkinite-(Ce) occurs mainly in syenites, alkaline to peralkaline granites and rhyolites, and fenites whereas perrierite-(Ce) is more common in metaluminous felsic igneous rocks. Few occurrences have been reported from igneous rocks of mafic affinity (Kallio 1967; Raade 1970; Azambre et al. 1987), and the only chemical analyses are of xenomorphic crystals of either chevkinite-(Ce) or perrierite-(Ce) associated with late-stage igneous amphiboles in tholeiitic dolerites of the Pyrenees (Azambre et al. 1987).

Chevkinite and perrierite are dimorphs (Ito 1967; Ito and Arem 1971), and distinguishing between them in rock samples has proved difficult as they have similar compositions and optical

properties (e.g., Jaffe et al. 1956; Bonatti 1959). Natural crystals have similar structures in the C2/m space group (Gottardi 1960; Yang et al. 2002), but diffraction data allow the two minerals to be differentiated by the □ angle which is 100◦ in chevkinites and 113◦ in perrierites (e.g., Haggerty and Mariano 1983). This is the most reliable way of distinguishing between natural chevkinite-(Ce) and perrierite-(Ce), but determining crystal structure can be difficult as many crystals are metamict, or form small grains that can only be located in thin sections with the aid of a microscope. As with many metamict minerals, crystal structure can be restored by annealing. Lima-de-Faria (1962) conducted the most complete series of heating experiments, in air and in nitrogen, on natural crystalline and metamict chevkinite and perrierite samples. Metamict chevkinite-(Ce) had the chevkinite structure after heating in nitrogen for 1 hour at 1000◦C, but on heating in air to 1000◦C, it formed perrierite-(Ce) and CeO_2. Crystalline chevkinite retained its structure on heating to 1300◦C. Metamict perrierite annealed with the perrierite structure, and both metamict and crystalline samples retained the perrierite structure on further heating. By contrast, a study of only slightly metamict chevkinite-(Ce) and perrierite-(Ce) from Virginia, found that chevkinite began to transform to perrierite on heating above 600◦C, and that both chevkinite and perrierite produced CeO_2 on heating to higher temperatures (Mitchell 1966).

To overcome the uncertainties in identifying natural chevkinite-(Ce) and perrierite-(Ce) based on their crystal structures, Macdonald and Belkin (2002) proposed a compositional discriminant based on a plot of CaO vs FeO* (total Fe as FeO). The discriminant was based on an extensive investigation of the compositional variations of the two minerals (Macdonald and Belkin 2002) and has been supported by subsequent studies (Belkin et al. 2009; Macdonald et al. 2009; Macdonald et al. 2012; Macdonald et al. 2013) that found that perrierite-(Ce) has less

FeO* and Ce_2O_3 and more CaO, Al_2O_3 and ZrO_2 than chevkinite-(Ce). These compilations lacked analyses of chevkinite group minerals from true mafic igneous rocks, the only analyses from mafic rocks being those reported by Azambre et al. (1987) of either chevkinite-(Ce) or perrierite-(Ce).

Here we show that chevkinite-(Ce) and perrierite-(Ce) are more common than has been supposed in tholeiitic intrusive rocks. We also present the first description of chevkinite/perrierite in lunar mare basalt. We describe the occurrence and composition of chevkinite and perrierite in mafic igneous rocks, and show that there are two distinct groups based on the amount of FeO*: a group with >8 wt% FeO* interpreted to be chevkinite-(Ce), and a group with <8 wt% FeO* interpreted to be perrierite-(Ce). The compositions of the high FeO* group span the line used to differentiate between chevkinite-(Ce) and perrierite-(Ce) so that diffraction data are necessary to discriminate between the dimorphs in this compositional range.

OCCURRENCE

Chevkinite/perrierite (c/p: chevkinite or perrierite identified by composition without confirmation of crystal structure) from mafic igneous rocks was first described and analyzed by Azambre et al. (1987) in tholeiitic dolerites from the Pyrenees, although occurrences in anorthositic gabbro (Kallio 1967) and a quartz-rich pegmatitic lens in anorthosite (Raade 1970) had been documented without textural relationships and the grains were not fully analyzed. In the Pyrenean samples, c/p forms xenomorphic microcrystals associated with late-stage igneous amphiboles in pegmatitic dolerite. Other accessory phases in the rock include zircon and allanite. The c/p described by Kallio (1967) was metamict, but was determined to be perrierite after

heating to 1000◦C for one hour. Similarly, the sample described by Raade (1970) was metamict but was determined to be perrierite after heating at 1000◦C for one day.

Accessory c/p has been found in eight suites of tholeiitic dolerite dikes and sills from Western Australia (Fig. 1 and Table 1) during an assessment of these rocks for geochronology. Mineral chemical analyses have been collected from crystals of c/p in five of these suites: 1) granophyre of the Hart Dolerite from the Kimberley region (Sheppard et al. 2012); 2) a sill of the Warakurna Large Igneous Province (Wingate et al. 2004) intruding the Eel Creek Formation on the northern edge of the Pilbara Craton (Rasmussen et al. 2012); 3) a sill intruding the Manganese Group at Woodie Woodie in the east Pilbara (Rasmussen and Fletcher 2004); 4) a dike of the Mundine Well dike swarm from the northern Gascoyne Province (Wingate and Giddings 2000); and 5) a dike of the Northampton swarm, interpreted to be equivalent to the Mundine Well swarm (Li et al. 2006), from the Pinjarra Orogen.

Two small grains of c/p have also been found in samples 11 and 227 of ca 3710 Ma-old lunar mare basalt 10047 from the Sea of Tranquillity. The rock is a subophitic basalt comprising mainly equant clinopyroxene (~45%), lath-shaped plagioclase (~30%), subhedral ilmenite (~15%), and interstitial cristobalite (Lovering and Ware 1970; Dence et al. 1970; Lovering et al. 1974; Beaty and Albee 1978; Rasmussen et al. 2008). Angular pockets of late-stage mesostasis contain Si-Al-K glass and minerals rich in K, Ba, U, Th, Zr, REE, Nb, P and Fe, including barian potassium feldspar, fayalite, pyroxferroite, troilite, native Fe, apatite, britholite, monazite, zirconolite, tranquillityite and baddeleyite. Two grains of c/p have now been found, one in fragment 11 (~20 μm) and one in 227 (~4 μm). Both grains are located in small pockets of mesostasis between plagioclase and clinopyroxene (227), and between plagioclase and

This is a preprint, the final version is subject to change, of the American Mineralogist (MSA)
Cite as Authors (Year) Title. American Mineralogist, in press.
(DOI will not work until issue is live.) DOI: http://dx.doi.org/10.2138/am-2014-4690

cristobalite (11). In backscattered electron (BSE) images, these grains are fresh and compositionally homogeneous (Fig. 2).

ANALYTICAL METHODS

Optical and scanning electron microscopy

Rocks containing c/p were examined in polished thin sections using optical and scanning electron microscopes (SEM). A JEOL 6400 SEM fitted with an Oxford Instruments Link Analytical Energy Dispersive X-ray detector (EDS) and BSE detector, and a TESCAN VEGA3 SEM fitted with an Oxford Instruments X-Max50 EDS and BSE detector, both located in the Centre for Microscopy, Characterisation and Analysis (CMCA) at the University of Western Australia (UWA), were used to locate crystals of c/p and other accessory phases with potential for U-Pb geochronology. The grains were identified based on their optical properties and characteristic X-ray spectra.

Electron microprobe analytical procedures

Selected c/p crystals were analyzed by electron microprobe (EMPA). Wavelength-dispersive analyses were collected at CMCA using an automated JEOL 8530F Hyperprobe fitted with five spectrometers. Operating conditions for analysis of c/p were 20 kV accelerating voltage, 50 nA beam current and a spot size of ~1 μm. Details of the EMPA analytical procedure

are given in Table 2. Background positions were selected according to the method of Williams (1996). X-ray acquisition and data reduction, including calculation of overlap factors based on measured standards, used Probe for EPMA software from Probe Software, Inc. Relative errors based on counting statistics are better than 1% for concentrations >5 wt%; 1-10% for concentrations 0.1-5 wt%; and >10% for concentrations <0.1 wt%. Crystals of c/p from heated samples (see below) were analyzed for major and minor elements by energy-dispersive analysis using the X-Max50 detector and AZtec software from Oxford Instruments.

Focused Ion Beam and Transmission Electron Microscope studies

Foils for transmission electron microscope (TEM) studies were cut from crystals of c/p located in polished thin sections. Focused ion beam (FIB) techniques using an FEI Helios NanoLab DualBeam instrument located at Adelaide Microscopy, the University of Adelaide, were used to prepare the foils. Areas selected for analysis were first coated with a strip of Pt ~1 μm thick to protect the surface, then trenches ~5 μm deep were milled on either side of the strip using a Ga ion beam with 30 kV voltage and 21 nA current. The foil was then cut away from the sample and welded to a Cu TEM grid with a Kleindiek Nanotechnik micromanipulator. The foils were thinned with the Ga ion beam at 30 kV and 0.28-0.92 nA, before cleaning at 5 kV and 47 pA, and polishing at 2 kV and 28 pA.

The structural and compositional properties of the foils at subnanometer scale were determined with TEM and associated analytical tools. TEM imaging, selected area electron diffraction (SAED) and energy-filtered TEM (EFTEM) studies were carried out using a JEOL 2100 instrument operating at 200 kV and equipped with an 11M pixel Gatan ORIUS digital

camera and Gatan Tridiem energy filter. For annealed samples, three zone axis images and SAED patterns were collected from crystalline phases. Interplanar distances and angles were measured from Digital Micrographs, and CaRIne Crystallography software was used to interpret the crystal structures.

PETROGRAPHY AND HABIT

Chevkinite/perrierite is most abundant in specimens from the dolerite sill from Woodie Woodie and from the sill intruding the Eel Creek Formation, while the largest grains have been found in the Hart Dolerite granophyre. These occurrences are described in more detail below. The specimens from Woodie Woodie comprise plagioclase laths (45-50%) 200 μm long on average with rare equant microphenocrysts ~500 μm across. The laths show normal zoning from labradorite cores to oligoclase rims and are fully or partially enclosed in clinopyroxene (~40%). The clinopyroxene is composed of intergrowths of pigeonite and augite, and both show normal zoning with 100Mg/(Mg+Fe), where Mg and Fe are cations calculated on the basis of six oxygen atoms, ranging from 70-75 in the cores to ~25 at the rims. Ilmenite (10%) and minor ferro-edenite or ferro-hornblende (1%), biotite (1%), orthoclase (1%) and quartz (1%) make up the remainder of the rock. Amphibole forms narrow rims on clinopyroxene as well as small grains in the rock matrix. Orthoclase and quartz form granophyric intergrowths in interstices between plagioclase laths. Accessory phases include zircon, baddeleyite, zirconolite, tranquillityite, c/p, monazite, apatite, thorite and allanite. Zirconolite, tranquillityite and c/p, in particular, are concentrated in the mesostasis. The rocks show evidence of minor alteration of clinopyroxene, sericitization of plagioclase and clouding of orthoclase. Chevkinite/perrierite is

present as red-brown, equant to elongate (10-20 μm), subhedral prismatic grains in the quartz-orthoclase mesostasis (Figs. 3a, 3b) that may also enclose small grains of amphibole or biotite, and other accessory phases. Most c/p grains show minor evidence of alteration, with material of lower atomic number developed around rims and along fractures (Fig. 3b). Chevkinite/perrierite is one of the last phases to crystallize along with orthoclase-quartz mesostasis and some other accessory phases enriched in incompatible elements (Figs. 3a, 3b).

The Eel Creek sill comprises augite and pigeonite crystals up to 2 mm across (~40%) enclosing or partially enclosing laths of plagioclase 1-2 mm long (45-50%). The plagioclase laths are zoned from labradorite to albite and are partly clouded by fine inclusions of sericite and epidote. Pigeonite shows minor alteration to intergrowths of secondary amphibole and very fine-grained opaques (Fig. 3d). Ilmenite constitutes ~10% of the rock, with traces of green-brown amphibole (~1%) and biotite (~1%), and granophyric quartz-orthoclase mesostasis (1-2%). Accessory minerals include apatite, zircon, zirconolite, baddeleyite, tranquillityite and c/p. Chevkinite/perrierite mostly forms equant to irregular crystals 10-20 μm across enclosed in green-brown amphibole on the margins of clinopyroxene crystals (Figs. 3d-f). The c/p grains may be surrounded by pronounced dark haloes in the amphibole (Fig. 3e). Less commonly, c/p forms grains within late-stage quartz-orthoclase mesostasis between plagioclase laths. In BSE images, some grains of c/p show subtle compositional zoning related to crystal faces, which is interpreted to be primary (Fig. 3f), and some grains have a distinctly mottled or patchy appearance possibly due to alteration or minor hydration of the original grains (Fig. 3f), while others appear fresh.

The Hart Dolerite comprises sills and dikes of dolerite and granophyre. The dolerite and granophyre are interpreted to form separate intrusions, although some field relationships suggest

that they are coeval (Sheppard et al. 2012). Chevkinite/perrierite was found in a sample from a slightly weathered sill of coarse-grained granophyre. It comprises ~50% albite laths up to 2 mm long, with interstitial micrographic intergrowths of quartz and orthoclase (20-25%), and ~20% of pale green hedenbergite. Ilmenite and ilvaite make up ~5%, while apatite, zircon, baddeleyite, zirconolite and c/p are accessories. Secondary Fe hydroxides are present throughout the sample. Chevkinite/perrierite forms poorly terminated prismatic crystals up to 400 μm long. These crystals are not pleochroic, but show core to rim color zoning from red-brown to yellow-brown (Fig. 4a). Optical properties other than color are difficult to determine because of masking, and metamictization. In BSE images, most grains show some evidence of alteration, with material of lower atomic number developed around rims and along fractures (Fig. 4b).

In mafic rocks, c/p are paragenetically late, crystallizating after the essential phases and synchronously with minor igneous hornblende and biotite, and/or quartz-orthoclase mesostasis.

COMPOSITION

Electron microprobe analyses of c/p from Western Australian dolerites and lunar sample 10047 are available in the Data Depository. Representative analyses are presented in Table 3. Despite metamictization and low-grade metamorphism, all analyses closely match the ideal formula for c/p $A_4BC_2D_2Si_4O_{22}$. For ease of comparison, cations have been allocated according to the scheme of Macdonald and Belkin (2002) which follows that of Parodi et al. (1994) for the dominant components.

Analyses with >4.3 apfu (atoms per formula unit) Si were rejected as they likely resulted from generation and detection of X-rays from adjacent phases. Analysis totals are mostly

239 between 98-100 wt%, indicating that despite being metamict the c/p grains are not hydrated (cf.
240 Yang et al. 2002). By contrast, analyses from grains of c/p showing a mottled appearance in BSE
241 images have low totals (~95-98 wt%), indicating minor hydration.
242 Despite evidence for alteration around grain margins and along fractures (Figs. 3b, 3f) most
243 c/p grains do not show compositional zoning in BSE images. Where analyzed, the alteration
244 areas are similar to unaltered grains, but on average have slightly more Si and less Fe, as well as
245 low totals (90-97 wt%). An exception is a prismatic crystal from the Hart Dolerite granophyre
246 that shows evidence for minor alteration along grain boundaries and fractures in BSE images
247 (Fig. 4b) but also shows variation of Fe and Ca in X-ray element distribution maps (Figs. 4c, 4d).
248 The grain has an Fe-depleted and Ca-enriched rim that does not coincide exactly with obvious
249 areas of alteration. The irregular outline of the Fe-rich core suggests that the compositional
250 zoning is related to alteration rather than igneous processes.
251 **A site**
252 Cation totals in the A site range from 3.908 to 4.186. The dominant cations are Ca (0.680-
253 1.596 apfu) and REE (2.336-3.145 apfu). Ce and La are the dominant REE, with appreciable Nd,
254 Pr and Sm. Y and Th are significant components at ~0.002-0.140 and ~0.000-0.176 apfu,
255 respectively. Abundances of Pb and U are mostly very low or below detection, while F, Na and
256 Sr were not detected in any analyses. The light REE are strongly fractionated, with La/Sm in the
257 range 12 to 109. The compositions of c/p from the Hart Dolerite granophyre are less fractionated
258 with La/Sm of 13-17. The heavy REE are less abundant: Eu, Ho, Tm and Lu were not detected in
259 any analyses, and Gd, Tb, Dy, Er and Yb have values close to their detection limits and large
260 relative errors (Table 2).

In grains from lunar mare basalt 10047, cation totals in the A site are 3.810-3.994, with 1.120-1.159 apfu Ca and 2.536-2.686 apfu REE. Y is more abundant (0.119-0.175 apfu) and Th less so (0.008-0.012 apfu) compared with the terrestrial samples. Light REE are unfractionated, with low La/Sm of ~4, while abundances of the heavy REE are again below or close to their detection limits.

C site

Cation totals in the C site range from 1.874 to 2.324, and the site is dominated (76-88%) by Al, Ti and Fe. Mn (0.009-0.025 apfu) and Mg (0.000-0.155 apfu) are both low, despite the mafic composition of the host rocks. The other significant component of the C site is Zr, in the range 0.092 to 0.406 apfu. Analyses from the Hart Dolerite granophyre have the highest Zr contents (average 0.270 apfu). Nb ranges from 0.006 to 0.046 apfu, and traces of Cr, Hf, Ta, W and P are also detected.

Analyses from lunar basalt 10047 have 1.873-2.141 cations in the C site, again dominated by Al, Ti and Fe. Zr and Nb are both significant with 0.247-0.274 and 0.112-0.273 apfu, respectively. Zr has a similar abundance to c/p from terrestrial rocks, but Nb is more abundant.

B, D and Tetrahedral sites

In all analyses, both terrestrial and lunar, the B site is completely filled by Fe^{2+} and the D site is completely filled by Ti. Si is the only cation allocated to the tetrahedral site. Si ranges from 3.949 to 4.227.

Comparison with chevkinite and perrierite from other lithologies

The most notable compositional feature of c/p from mafic rocks is their Zr content which ranges from 0.092 to 0.406 apfu and falls between the Zr contents of c/p from most igneous, metamorphic and hydrothermal rocks tabulated by Macdonald and Belkin (2002), Vlach and Gualda (2007), Belkin et al. (2009), Macdonald et al. (2009) and Macdonald et al. (2012), and Zr-rich analyses reported by Parodi et al. (1994) and Carlier and Lorand (2008). Only six analyses of perrierite-(Ce) from the Mushugai-Khuduk carbonatite complex (Macdonald et al. 2009) have 0.2-0.4 apfu Zr, whereas 66% of analyses from mafic rocks fall within this range. There is a strong positive correlation between Ca+Sr and Zr in c/p (Fig. 5a), with analyses from mafic samples dominating the spread in Zr content between 0.1 and 0.4 apfu. Similarly, there is a well-defined negative correlation between $Ca+Sr+Ti_C+Zr$ and ΣREE in c/p (Fig. 5b), with the analyses from mafic rocks dominant between 1.5 and 3 apfu $Ca+Sr+Ti_C+Zr$.

Macdonald and Belkin (2002) developed a triangular plot of elements enriched in perrierite (Ca, Sr, Mg, Al) against elements enriched in chevkinite (Fe, LREE) showing the fields of chevkinite and perrierite from various igneous rock types. On this plot, the analyses of c/p from tholeiitic dolerites overlap the fields of mafic and intermediate igneous rocks, calcic granites and more evolved rocks (Fig. 6). The analyses define two lobes: one parallel to the perrierite trend of Ca enrichment and the other showing Fe enrichment more typical of chevkinite.

CHEVKINITE OR PERRIERITE

CaO versus FeO*

Macdonald and Belkin (2002) used the Ca-enrichment trend of perrierite and the Fe-enrichment trend of chevkinite to develop a chemical discriminator for the two minerals based on plots of CaO versus FeO*. The line of discrimination has been modified slightly in subsequent compilations (Belkin et al. 2009; Macdonald et al. 2009; Macdonald et al. 2012) but has been found to be valid. In c/p from mafic samples, FeO* ranges from ~6.5 to 10.5 wt% and CaO from 3.4 to 7.4 wt%. This compositional range straddles the line for chemical demarcation of chevkinite and perrierite (Fig. 7a). Excepting the crystal of c/p from the Hart Dolerite that shows zoning in Ca and Fe (Fig. 4), individual analyses fall into two groups on a plot of CaO versus FeO*: those with >8 wt% FeO* and those with <8 wt% FeO*, although the CaO contents of the two groups overlap between ~4.5 and 6.0 wt%. Within individual grains, FeO* generally varies by <0.5 wt%, while CaO may vary by 1-2 wt%.

Intragrain and intergrain relationships may be demonstrated by analyses of different grains of c/p from within the same sample of dolerite from Woodie Woodie (Fig. 7b). Of the nine grains analyzed, three have >8 wt% FeO*, while the remainder have <8 wt% FeO* and plot in the perrierite field. Of the three high-Fe grains, grain C analyses plot mostly in the chevkinite field, while grains F and I plot in the perrierite field. All of these crystals appear fresh, apart from obvious minor alteration along fractures and grain boundaries, and have analysis totals between 98.5 and 100 wt%. All of the grains are located in the quartz-orthoclase mesostasis between plagioclase laths. Grain C (high FeO*) is adjacent to a small grain of biotite, as is grain D (low FeO*). Analyses of seven grains from the Eel Creek sill include three with high Fe that plot in the chevkinite field, and four with low Fe that plot in the perrierite field. Four grains from the Hart Dolerite include three with high Fe and one with low Fe, but all plot in the perrierite field, while grains from Mundine Well have high Fe, but one plots in the chevkinite field and one in

the perrierite field, as do the analyses reported by Azambre et al. (1987). Analyses of grains from the Northampton dikes and the Moon fall in the high FeO* group within the perrierite field. The Macdonald and Belkin (2002) discriminator indicates that the low FeO* group is perrierite, but the high FeO* group includes both chevkinite and perrierite. However, the presence of two groups with distinct Fe contents suggests two distinct minerals, with the high-FeO* group being chevkinite-(Ce) and the low-FeO* group being perrierite-(Ce). Crystal structural information is required to confirm this suggestion.

Structural information

The crystal structure of the two compositional groups of c/p from the tholeiitic dolerites was investigated by electron diffraction using TEM. The very small grain size necessitated preparation of TEM foils by cutting a slice from grains using a FIB instrument. Chevkinite/perrierite from the Eel Creek dolerite was found to be completely amorphous (metamict), necessitating heating to anneal the c/p prior to structural analysis. A sample of Eel Creek dolerite was heated in air at 950◦C for one day (cf. Raade 1970), and three polished thin sections were prepared from it. TEM foils were made from c/p with <8 wt% FeO* located in these sections. TEM imaging, Electron Energy Loss Spectroscopy, and element mapping by EFTEM showed that the c/p had recrystallized to c/p, Ce oxide and a Ti-rich phase (Fig. 8). Measurement of electron diffraction patterns and crystal structure analysis showed that the annealed c/p contained perrierite.

Samples from Woodie Woodie, Mundine Well and the Hart Dolerite were in short supply, so three samples of dolerite from a Northampton dike that SEM/EDS analysis had shown to contain

c/p that plots in the perrierite field, but with >8 wt% FeO* (Fig. 7a), were selected for examination. A less severe heating regime was chosen in order to prevent breakdown of the c/p into multiple phases. The samples were heated in air at 800◦C for 30 minutes and foils were prepared from c/p found in these samples. TEM imaging showed that the c/p was a mixture of stellate aggregates of acicular crystals in a featureless background (Fig. 9a). The structure derived from SAED analysis of the crystals (Fig. 9b) corresponds with the crystal structure of chevkinite-(Ce) reported by Mitchell (1966), while the background is amorphous (Fig. 9c).

DISCUSSION

Occurrence

Chevkinite-(Ce) and perrierite-(Ce) are common, although not abundant, accessory minerals in eight suites of tholeiitic dolerites from Western Australia, and are likely to be more common in mafic rocks than has been previously recognized. They occur in geographically, geologically and geochronologically distinct suites (Fig. 1), and are found with a range of other Ti-Zr and REE accessory minerals. They crystallize late in the paragenetic sequence, with minor igneous amphibole and/or quartz-orthoclase mesostasis, and are a significant host of REE in these rocks being more common than monazite or allanite. Grains are mostly 10-20 μm, and BSE imaging and EDS analysis are most effective aids in their identification.

Chevkinite/perrierite is a rare accessory phase in mesostasis in lunar mare basalt 10047 (Fig. 2), and may be more common in lunar rocks also. No diffraction data were obtained from c/p in the lunar samples. Analyses of a grain in 10047, 227 have >8 wt% FeO* and this phase is

374 interpreted to be chevkinite-(Ce); however, a single analysis of a small crystal in 10047, 11 has
375 7.83 wt% FeO* and could be either chevkinite-(Ce) or perrierite-(Ce).
376
377 **Composition**
378
379 The composition of c/p in mafic rocks is distinctive and has appreciably more Zr than found
380 in most other common rock types. It occupies sparsely populated fields in plots of Ca+Sr vs Zr
381 and $Ca+Sr+Ti_C+Zr$ vs ΣREE, and most notably in plots of CaO vs FeO* where the compositions
382 straddle the boundary between chevkinite and perrierite (Figs. 5, 7).
383
384 **Chevkinite or perrierite?**
385
386 The compositions of c/p grains analyzed from tholeiitic dolerites generally fall into two
387 groups in a plot of CaO vs FeO*: one group with >8 wt% FeO* that merges with the chevkinite
388 field and one with <8 wt% FeO* within the perrierite field, although the two groups overlap in
389 CaO content (Fig. 7). An annealed grain with >8 wt% FeO* that plots in the perrierite field has
390 been shown by SAED to have the chevkinite structure, suggesting that the high-Fe group
391 comprises chevkinite-(Ce). According to SAED analysis, an annealed low-Fe grain from the
392 perrierite field has the perrierite structure, but these results are inconclusive because both
393 perrierite and chevkinite are known to break down to perrierite and CeO_2 on heating (Lima-de-
394 Faria 1962; Mitchell 1966). The low-Fe group is interpreted to comprise perrierite, in agreement
395 with its location in the CaO vs FeO* discriminant plot.

Analyses of individual grains of c/p from samples of the Hart Dolerite, the dolerite intruding the Eel Creek formation and the dolerite from Woodie Woodie fall within both the high-Fe and low-Fe groups (Fig. 7). Therefore, if the two groups represent chevkinite-(Ce) and perrierite-(Ce), both dimorphs can occur within the same rock sample and maintain their compositional differences regardless of subsequent metamictization.

Most of the crystals of c/p that have been analyzed show some effects of alteration along grain boundaries and fractures, and some have a mottled appearance in BSE images (Fig. 3f). It is likely that some of the spread in compositions between the high-Fe and low-Fe groups is due to alteration and minor hydration. This is particularly true of a crystal from the Hart Dolerite that has an irregular Fe-rich core with a composition in the chevkinite field, and a more Ca-rich rim whose composition plots in the perrierite field (Fig. 4). If the composition controls the crystal structure, both dimorphs may be present within the one grain.

Discrimination

Following an investigation of a range of synthetic minerals with chevkinite or perrierite structures, Ito (1967) concluded that the transition from chevkinite to perrierite is controlled by the average ionic radii of cations in the A and B+C sites in the crystal structure. The dimorphs are separated by a field in which both may coexist.

Calculations of the average ionic radii of the A and B+C sites for analyses of c/p for the two compositional groups recognized in mafic rocks shows that the phase boundary defined by Ito (1967) does not hold, probably due to differences in allocating cations to sites in natural samples, and differences in the ionic radii used for the calculation, but nonetheless the two groups have

distinct values of average ionic radii. As with synthetic samples, perhaps there is a compositional field where both dimorphs can coexist.

The two groups can be distinguished by their Fe and Al contents: in the chevkinite group, the high Fe is matched by low Al, whereas the perrierite group (low Fe) has higher Al. The discriminant value of 8 wt% FeO* is applicable to the analyses from mafic rocks reported herein, and to the majority of analyses reported by Macdonald and Belkin (2002), Belkin et al. (2009), Macdonald et al. (2009), Macdonald et al. (2012). However, there are exceptions and there is no universally applicable discriminant based on composition for distinguishing between the two dimorphs. Crystal structure data are required for final identification.

IMPLICATIONS

The occurrence of both chevkinite-(Ce) and perrierite-(Ce) in single hand specimens from the same tholeiitic intrusion suggests that pockets of late-stage melt in these rocks have subtle variations, and that these variations control which of the dimorphs is formed. Understanding these heterogeneities may clarify the effects of ionic radii and melt composition on the crystallization of chevkinite group minerals, and provide insights into processes of igneous crystallization and fractionation. Future investigations of the crystallization of chevkinite-(Ce) and perrierite-(Ce) in tholeiitic intrusions should target young samples to avoid the problems of radiation-induced crystal damage.

Chevkinite-(Ce) and perrierite-(Ce) contain about 35-40 wt% REE, and significant amounts of other incompatible elements, and are the most abundant hosts of REE in tholeiitic dolerite and gabbro intrusions. Understanding the geochemical behaviour of the incompatible elements is

particularly important in petrogenetic studies of igneous rock systems and recognition of phases such as chevkinite-(Ce) and perrierite-(Ce) in mafic intrusives can help refine models for the origins of these rock suites. Many of the samples described in this study are from recognized Large Igneous Provinces (LIPs), so better understanding of the intrusions themselves can contribute to models for the origins of LIPs and associated mantle plumes.

ACKNOWLEDGEMENTS

Len Green from Adelaide Microscopy demonstrated his expertise in FIB in preparing the foils for TEM analysis. We thank Gary Lofgren (Lunar Sample Curator) and the Lyndon B. Johnson Space Centre (NASA) for their generous support and access to samples from the Apollo 11 mission. We thank the Smithsonian National Museum of Natural History for their assistance in providing microbeam reference samples. The authors acknowledge the facilities and technical assistance of the Australian Microscopy & Microanalysis Research Facility at the Centre for Microscopy, Characterisation & Analysis, UWA, and Adelaide Microscopy, University of Adelaide, facilities funded by the Universities, State and Commonwealth Governments. The manuscript was improved following reviews by Ray Macdonald and Panseok Yang and editorial handling by Anton Chakhmouradian.

REFERENCES

Azambre, B., Rossy, M., and Lago, M. (1987) Caractéristiques pétrologiques des dolérites tholéiitiques d'âge triasique (ophites) du domaine pyrénéen. Bulletin de Minéralogie, 110, 379-396.

466 Beaty D.W. and Albee A.L. (1978) Comparative petrology and possible genetic relations among
467 the Apollo 11 basalts. Proceedings of the 9th Lunar and Planetary Science Conference,
468 Geochimica et Cosmochimica Acta (Supplement 9), 359–463.
469 Belkin, H.E., Macdonald, R., and Grew, E.S. (2009) Chevkinite-group minerals from granulite-
470 facies metamorphic rocks and associated pegmatites of East Antarctica and South India.
471 Mineralogical Magazine, 73, 149-164.
472 Bonatti, S. (1959) Chevkinite, perrierite and epidotes. American Mineralogist, 44, 115-137.
473 Carlier, G., and Lorand, J-P. (2008) Zr-rich accessory minerals (titanite, perrierite, zirconolite,
474 baddeleyite) record strong oxidation associated with magma mixing in the south Peruvian
475 potassic province. Lithos, 104, 54-70.
476 Dence M.R., Douglas J.A.V., Plant A.G., and Traill R.J. (1970) Petrology, mineralogy and
477 deformation of Apollo 11 samples. Proceedings of the Apollo 11 Lunar Science Conference,
478 Geochimica et Cosmochimica Acta (Supplement 1), 315–340.
479 Gottardi, G. (1960) The crystal structure of perrierite. American Mineralogist, 45, 1-14.
480 Ito, J. (1967) A study of chevkinite and perrierite. American Mineralogist, 52, 1094-1104.
481 Ito, J. and Arem, J.E. (1971) Chevkinite and perrierite: Synthesis, crystal growth and
482 polymorphism. American Mineralogist, 56, 307-319.
483 Jaffe, H.W., Evans, H.T. Jr, and Chapman, R.W. (1956) Occurrence and age of chevkinite from
484 the Devil's Slide fayalite-quartz syenite near Stark, New Hampshire. American
485 Mineralogist, 41, 474-487.
486 Jiang, N. (2006) Hydrothermal alteration of chevkinite-(Ce) in the Shuiquangou syenitic
487 intrusion, northern China. Chemical Geology, 227, 100-112.

Haggerty, S.E. and Mariano, A.N. (1983) Strontian-loparite and strontio-chevkinite: Two new minerals in rheomorphic fenites from the Paraná Basin carbonatites, South America. Contributions to Mineralogy and Petrology, 84, 365-381.

Kallio, P. (1967) Perrieritie from Mäntyharju, Finland. Comptes Rendus de la Sosiété géologique de Finlande, 39, 41-43.

Li, X.H., Li, Z.X., Wingate, M.T.D., Chung, S.L., Liu, Y., Lin, G.C., and Li, W.X. (2006) Geochemistry of the 755 Ma Mundine Well dike swarm, northwestern Australia: Part of a Neoproterozoic mantle superplume beneath Rodinia? Precambrian Research, 146, 1-15.

Lima-de-Faria, J. (1962) Heat treatment of chevkinite and perrierite. Mineralogical Magazine, 33, 42-47.

Lovering J.F. and Ware N.G. (1970) Electron probe microanalyses of minerals and glasses in Apollo 11 lunar samples. Proceedings of the Apollo 11 Lunar Science Conference, Geochimica et Cosmochimica Acta (Supplement 1), 633–654.

Lovering, J.F., Wark, D.A., Gleadow, A.J.W., and Britten, R. (1974) Lunar monazite: A late-stage (mesostasis) phase in mare basalt. Earth and Planetary Science Letters, 21, 164-168.

Macdonald, R. and Belkin, H.E. (2002) Compositional variation in minerals of the chevkinite group. Mineralogical Magazine, 66, 1075-1098.

Macdonald, R., Bagiński, B., Dzierżanowski, P., Fettes, D.J., and Upton, B.G.J. (2013) Chevkinite-group minerals in UK Palaeogene granites: Underestimated REE-bearing accessory phases. Canadian Mineralogist, 51, 333-347.

Macdonald, R., Bagiński, B., Kartashov, P., Zozulya, D., and Dzierżanowski, P. (2012) Chevkinite-group minerals from Russia and Mongolia: new compositional data from metasomatites and ore deposits. Mineralogical Magazine, 76, 535-549.

511 Macdonald, R., Belkin, H.E., Wall, F., and Bagiński, B. (2009) Compositional variation in the
512 chevkinite group: new data from igneous and metamorphic rocks. Mineralogical Magazine,
513 73, 777-796.
514 Macdonald, R., Marshall, A.S., Dawson, J.B., Hinton, R.W., and Hill, P.G. (2002) Chevkinite-
515 group minerals from salic volcanic rocks of the East African rift. Mineralogical Magazine,
516 66, 287-299.
517 Mitchell, R.S. (1966) Virginia metamict minerals: perrierite and chevkinite. American
518 Mineralogist, 51, 1394-1405.
519 Parodi, G.C., Della Ventura, G., Mottana, A., and Raudsepp, M. (1994) Zr-rich non metamict
520 perrierite-(Ce) from holocrystalline ejecta in the Sabatini volcanic complex (Latium, Italy).
521 Mineralogical Magazine, 58, 607-613.
522 Prol-Ledesma, R.-M., Melgarejo, J.C., and Martin, R.F. (2012) The El Muerto “NYF” granitic
523 pegmatite, Oaxaca, Mexico, and its striking enrichment in allanite-(Ce) and monazite-(Ce).
524 Canadian Mineralogist, 50, 1055-1076.
525 Raade, G. (1970) Perrierite from the Sogndal anorthosite, south Norway. Contributions to the
526 mineralogy of Norway, 43, 241-243.
527 Rasmussen, B., and Fletcher, I.R. (2004) Zirconolite: A new U-Pb chronometer for mafic
528 igneous rocks. Geology, 32, 785-788.
529 Rasmussen, B., Fletcher, I.R., Gregory, C.J., Muhling, J.R., and Suvorova, A.A. (2012)
530 Tranquillityite: The last lunar mineral comes down to Earth. Geology, 40, 83-86.
531 Rasmussen, B., Fletcher, I.R., and Muhling, J.R. (2008) Pb/Pb geochronology, petrography and
532 chemistry of Zr-rich accessory minerals (zirconolite, tranquillityite and baddeleyite) in mare
533 basalt 10047. Geochimica et Cosmochimica Acta, 72, 5799-5818.

534 Sheppard, S., Page, R.W., Griffin, T.J., Rasmussen, B., Fletcher, I.R., Tyler, I.M., Kirkland,
535 C.L., Wingate, M.T.D., Hollis, J.A., and Thorne, A.M. (2012) Geochronological and
536 isotopic constraints on the tectonic setting of the c. 1800 Ma Hart Dolerite and the
537 Kimberley and Speewah Basins, northern Western Australia. Geological Survey of Western
538 Australia, Record 2012/7, 34 pp.
539 Troll, V.R., Sachs, P.M., Schmincke, H.-U., and Sumita, M. (2003) The REE-Ti mineral
540 chevkinite in comenditic magmas from Gran Canaria, Spain: a SYXRF-probe study.
541 Contributions to Mineralogy and Petrology, 145, 730-741.
542 Vlach, S.R.F., and Gualda, G.A.R. (2007) Allanite and chevkinite in A-type granites and syenites
543 of the Graciosa Province, southern Brazil. Lithos, 97, 98-121.
544 Williams, C.T. (1996) Analysis of rare earth minerals. In Rare Earth Minerals: Chemistry,
545 Origin and Ore Deposits (eds. A.P. Jones, F. Wall, C.T. Williams), Chapman and Hall, pp.
546 327-348.
547 Wingate, M.T.D., and Giddings, J.W. (2000) Age and palaeomagnetism of the Mundine Well
548 dike swarm, Western Australia: implications for an Australia-Laurentia connection at 755
549 Ma. Precambrian Research, 100, 335-357.
550 Wingate, M.T.D., Pirajno, F., and Morris, P.A. (2004) Warakurna large igneous province: A
551 new Mesoproterozoic large igneous province in west-central Australia. Geology, 32, 105-
552 108.
553 Yang, Z., Fleck, M., Smith, M., Tao, K., Song, R., and Zhang, P. (2002) The crystal structure of
554 natural Fe-rich chevkinite-(Ce). European Journal of Mineralogy, 14, 969-975.

555

556 TABLE 1. Western Australian localities of tholeiitic dikes and sills containing chevkinite-
557 perrierite

Location (Fig. 1)	Description	Age (M.a.)	Samples*
1	Hart Dolerite: granophyric sill intruding the Paleoproterozoic Speewah Group (Hart LIP†)	1795	113574; (04-121)
2	Sill intruding the Proterozoic Eel Creek Formation (Warakurna LIP)	1065	210508; (09-09)
3	Sill intruding the Mesoproterozoic Manganese Group at Woodie Woodie	525	WD401 & WD410; (04-13)
4	Dike of the Mundine Well Suite	755	712; (04-13H&J)
5	Sill intruding the Proterozoic Badgeradda Group	-	MUR18A
6	Dike of the Northampton Suite interpreted to be equivalent to the Mundine Well Suite	-	NH02
7	Dike of the Gnowangerup Suite intruding the Paleoproterozoic Stirling Range formation (Marnda Moorn LIP)	1210	
8	Cunderline Sill intruding the Paleoproterozoic Mount Barren Group	-	

558 *The first-listed numbers are field numbers; numbers in parentheses refer to epoxy mounts of c/p
559 crystals drilled from polished thin sections of field samples. Letters refer to individual grains
560 within the epoxy mount. So 04-13H refers to grain H in mount 04-13 derived from field sample
561 712.
562 †LIP: Large Igneous Province.
563

564
565 TABLE 2. Analytical conditions and detection limits for EMPA.

Element	X-Ray Line	Diffraction crystal	Count time (s)*	Detection limit (wt%)	Standard†
Si	Kα	TAP	50	0.005	wollastonite
Ti	Kα	PET	50	0.007	rutile
Zr	Lα	PET	50	0.019	CZ3 zircon
Hf	Lα	LIF	100	0.031	CZ3 zircon
Th	Mα	PET	100	0.014	ThO_2
U	Mβ	PET	100	0.025	U metal
Al	Kα	TAP	50	0.005	corundum
Cr	Kα	LIF	50	0.013	Cr metal
Y	Lα	PET	100	0.019	YPO_4
La	Lα	LIF	100	0.046	$LaPO_4$
Ce	Lα	LIF	50	0.062	$CePO_4$
Pr	Lβ	LIF	100	0.072	$PrPO_4$
Nd	Lβ	LIF	100	0.063	$NdPO_4$
Sm	Lβ	LIF	100	0.067	$SmPO_4$
Gd	Lβ	LIF	100	0.074	$GdPO_4$
Tb	Lβ	LIF	100	0.026	$TbPO_4$
Dy	Lα	LIF	100	0.022	$DyPO_4$
Er	Lα	LIF	100	0.014	$ErPO_4$
Yb	Lα	LIF	100	0.016	$YbPO_4$
Mg	Kα	TAP	100	0.005	forsterite
Ca	Kα	PET	50	0.005	wollastonite
Mn	Kα	LIF	50	0.012	spessartine
Fe	Kα	LIF	50	0.012	magnetite
Pb	Mα	PET	100	0.020	crocoite
P	Kα	TAP	50	0.006	$LaPO_4$
Nb	Lα	PET	100	0.012	$CaNb_2O_6$
Ta	Lα	LIF	100	0.026	$MnTa_2O_6$
W	Lα	LIF	100	0.027	scheelite

566 *Peak count time. The same count time was divided between the high and low background
567 positions.
568 †REE phosphate and magnetite standards from Smithsonian National Museum of Natural
569 History #NMNH168484-168499, NMNH2566.
570

571

572 TABLE 3. Representative analyses of chevkinite/perrierite from tholeiitic dolerites and lunar
573 basalt.
574

	Hart Dolerite				Eel Creek		
SAMPLE	04-121D3	04-121D6	04-121D7	04-121H2	04-121I3	09-09C2	09-09D1
SiO_2	20.32	20.45	19.95	21.30	20.89	20.74	20.76
TiO_2	19.88	19.66	19.60	20.66	20.31	17.37	17.85
ZrO_2	2.42	2.54	2.41	3.83	2.66	0.96	3.41
HfO_2	0.05	0.10	0.09	0.13	0.10	b.d.	0.12
ThO_2	0.80	0.81	0.82	0.45	0.97	1.12	0.66
UO_2	b.d.	b.d.	0.01	b.d.	0.03	b.d.	0.04
Al_2O_3	0.62	0.68	0.60	2.03	0.61	3.35	2.82
Cr_2O_3	b.d.	b.d.	b.d.	b.d.	b.d.	b.d.	b.d.
Y_2O_3	0.87	0.82	0.92	0.78	0.91	0.81	0.58
La_2O_3	10.14	10.04	9.93	9.80	9.98	14.01	13.53
Ce_2O_3	18.79	18.37	18.55	17.40	18.53	21.24	19.39
Pr_2O_3	1.81	1.74	1.76	1.62	1.84	1.60	1.44
Nd_2O_3	6.16	6.11	6.21	5.38	6.09	4.49	4.12
Sm_2O_3	0.73	0.75	0.80	0.63	0.78	0.44	0.38
Gd_2O_3	0.32	0.25	0.34	0.15	0.44	0.21	0.24
Tb_2O_3	b.d.	0.07	b.d.	0.02	0.05	b.d.	b.d.
Dy_2O_3	0.26	0.26	0.28	0.20	0.26	0.18	0.16
Er_2O_3	0.10	0.09	0.09	0.09	0.09	0.09	0.08
Yb_2O_3	0.04	0.04	0.03	0.09	0.03	0.07	0.05
MgO	0.03	0.00	0.03	0.03	0.02	0.52	0.35
CaO	5.04	5.74	5.04	7.20	5.46	3.38	4.76
MnO	0.10	0.14	0.09	0.08	0.09	0.06	0.06
FeO*	9.11	6.85	8.88	7.12	9.19	7.54	6.97
PbO	b.d.	b.d.	b.d.	b.d.	0.04	b.d.	b.d.
P_2O_5	0.14	0.14	0.02	0.17	0.12	0.13	0.21
Nb_2O_5	0.41	0.45	0.14	0.23	0.48	0.15	0.31
Ta_2O_5	0.03	b.d.	0.43	b.d.	0.06	b.d.	b.d.
WO_3	b.d.	b.d.	0.03	0.05	0.08	b.d.	b.d.
TOTAL	98.17	96.10	97.05	99.44	100.11	98.46	98.29

575 b.d. = below detection limit. FeO* = total Fe calculated as FeO.
576

577

578 Cations based on 22 oxygens

Si	4.065	4.140	4.048	4.052	4.083	4.148	4.099
Ti	2.991	2.994	2.990	2.956	2.986	2.613	2.651
Zr	0.236	0.251	0.239	0.355	0.254	0.094	0.328
Hf	0.003	0.006	0.005	0.007	0.005	0.000	0.007
Th	0.037	0.037	0.038	0.019	0.043	0.051	0.030
U	0.000	0.000	0.000	0.000	0.001	0.000	0.002
Al	0.147	0.163	0.144	0.455	0.140	0.791	0.657
Cr	0.000	0.000	0.000	0.000	0.000	0.000	0.000
Y	0.093	0.088	0.100	0.079	0.095	0.086	0.061
La	0.748	0.750	0.743	0.688	0.720	1.033	0.986
Ce	1.376	1.362	1.378	1.212	1.326	1.555	1.402
Pr	0.132	0.129	0.130	0.112	0.131	0.116	0.103
Nd	0.440	0.442	0.450	0.365	0.425	0.321	0.290
Sm	0.051	0.053	0.056	0.042	0.052	0.030	0.026
Gd	0.021	0.017	0.023	0.009	0.028	0.014	0.016
Tb	0.000	0.005	0.000	0.001	0.003	0.000	0.000
Dy	0.017	0.017	0.018	0.012	0.017	0.012	0.010
Er	0.006	0.006	0.006	0.005	0.005	0.006	0.005
Yb	0.003	0.003	0.002	0.005	0.002	0.004	0.003
Mg	0.008	0.000	0.010	0.008	0.006	0.155	0.103
Ca	1.080	1.246	1.096	1.468	1.143	0.723	1.008
Mn	0.018	0.023	0.015	0.013	0.015	0.010	0.010
Fe	1.524	1.161	1.507	1.133	1.503	1.262	1.152
Pb	0.000	0.000	0.001	0.000	0.002	0.000	0.000
P	0.024	0.024	0.024	0.027	0.020	0.022	0.035
Nb	0.037	0.042	0.039	0.020	0.043	0.014	0.028
Ta	0.002	0.000	0.001	0.000	0.003	0.000	0.000
W	0.000	0.000	0.000	0.001	0.001	0.000	0.000
TOTAL	13.059	12.959	13.063	13.044	13.052	13.060	13.012

579

580 TABLE 3 contd. Representative analyses of chevkinite/perrierite from tholeiitic dolerites and
581 lunar basalt.
582

	Eel Creek		Woodie Woodie				
SAMPLE	09-09G2	09-09M2	04-13A1	04-13B1	04-13C4	04-13F4	04-13G3
SiO_2	20.52	19.51	20.97	21.35	20.41	20.98	21.46
TiO_2	17.62	18.46	18.41	17.91	18.13	18.95	18.86
ZrO_2	1.16	1.06	2.79	2.61	1.35	1.94	3.39
HfO_2	0.05	0.05	0.12	0.23	0.09	0.05	0.21
ThO_2	2.68	1.79	0.80	3.24	3.25	2.86	1.10
UO_2	0.12	0.05	0.04	0.03	0.07	0.07	b.d.
Al_2O_3	0.94	0.85	3.01	3.58	1.01	0.87	2.82
Cr_2O_3	0.03	b.d.	b.d.	b.d.	b.d.	b.d.	b.d.
Y_2O_3	1.16	1.08	0.54	0.43	0.69	0.40	0.09
La_2O_3	10.48	11.13	13.63	11.77	12.72	11.24	13.81
Ce_2O_3	18.59	21.00	20.11	19.16	20.32	19.60	19.53
Pr_2O_3	1.87	1.78	1.40	1.45	1.49	1.72	1.23
Nd_2O_3	6.25	5.92	3.44	4.07	4.25	4.95	2.79
Sm_2O_3	0.89	0.89	0.29	0.38	0.46	0.53	0.15
Gd_2O_3	0.38	0.32	b.d.	0.11	0.16	0.10	b.d.
Tb_2O_3	0.07	b.d.	b.d.	b.d.	0.03	b.d.	b.d.
Dy_2O_3	0.31	0.29	0.10	0.08	0.14	0.17	0.03
Er_2O_3	0.11	0.09	0.07	0.04	0.05	0.07	b.d.
Yb_2O_3	0.04	0.04	0.06	0.06	0.03	b.d.	b.d.
MgO	0.24	0.18	0.32	0.38	0.29	0.29	0.27
CaO	3.31	3.05	5.38	5.65	3.67	4.71	6.18
MnO	0.08	0.07	0.06	0.07	0.09	0.09	0.07
FeO*	10.01	9.58	7.25	6.73	10.03	9.13	7.00
PbO	0.08	0.03	b.d.	b.d.	b.d.	b.d.	b.d.
P_2O_5	0.14	0.12	0.14	0.14	0.12	0.13	0.12
Nb_2O_5	0.20	0.22	0.13	0.08	0.28	0.47	0.13
Ta_2O_5	b.d.	b.d.	b.d.	b.d.	b.d.	b.d.	b.d.
WO3	0.06	0.09	0.04	0.04	0.12	0.08	0.05
TOTAL	97.39	97.65	99.10	99.59	99.25	99.40	99.29

583 b.d. = below detection limit. FeO* = total Fe calculated as FeO.
584

585

586 Cations based on 22 oxygens

Si	4.228	4.056	4.089	4.137	4.141	4.174	4.132
Ti	2.731	2.886	2.699	2.611	2.765	2.835	2.730
Zr	0.116	0.107	0.266	0.246	0.133	0.188	0.318
Hf	0.003	0.003	0.007	0.012	0.005	0.003	0.012
Th	0.126	0.085	0.036	0.143	0.150	0.129	0.048
U	0.005	0.002	0.002	0.001	0.003	0.003	0.000
Al	0.228	0.207	0.693	0.819	0.242	0.203	0.641
Cr	0.005	0.000	0.000	0.000	0.000	0.000	0.000
Y	0.127	0.120	0.056	0.044	0.075	0.042	0.009
La	0.796	0.854	0.981	0.842	0.952	0.825	0.981
Ce	1.403	1.598	1.436	1.360	1.509	1.427	1.376
Pr	0.140	0.135	0.099	0.103	0.110	0.124	0.086
Nd	0.460	0.439	0.239	0.282	0.308	0.351	0.192
Sm	0.063	0.064	0.020	0.025	0.032	0.036	0.010
Gd	0.026	0.022	0.000	0.007	0.011	0.007	0.000
Tb	0.004	0.000	0.000	0.000	0.002	0.000	0.000
Dy	0.021	0.019	0.006	0.005	0.009	0.011	0.002
Er	0.007	0.006	0.004	0.002	0.003	0.005	0.000
Yb	0.003	0.002	0.003	0.003	0.002	0.000	0.000
Mg	0.072	0.057	0.094	0.109	0.088	0.086	0.079
Ca	0.730	0.680	1.124	1.173	0.797	1.003	1.275
Mn	0.015	0.013	0.010	0.011	0.015	0.014	0.012
Fe	1.725	1.667	1.181	1.092	1.701	1.519	1.127
Pb	0.004	0.002	0.000	0.000	0.000	0.000	0.000
P	0.024	0.020	0.024	0.023	0.021	0.022	0.020
Nb	0.019	0.020	0.011	0.007	0.026	0.042	0.011
Ta	0.000	0.000	0.000	0.000	0.000	0.000	0.000
W	0.001	0.002	0.001	0.001	0.002	0.001	0.001
TOTAL	13.082	13.066	13.081	13.058	13.102	13.050	13.062

587

TABLE 3 contd. Representative analyses of chevkinite/perrierite from tholeiitic dolerites and lunar basalt.

	Woodie Woodie		Mundine Well		Moon		
SAMPLE	WD410-1B	WD410-1C	04-13H1	04-13J3	10047-222A	10047-11A	10047-11E
SiO_2	19.31	19.59	20.56	20.20	22.28	19.85	19.96
TiO_2	18.03	18.24	17.70	16.35	19.94	17.82	17.71
ZrO_2	1.56	1.61	2.25	1.70	2.68	2.83	2.80
HfO_2	0.07	0.11	0.12	0.16	0.21	0.19	0.22
ThO_2	2.15	2.72	b.d.	1.65	0.18	0.26	0.25
UO_2	0.08	0.04	0.03	0.04	b.d.	b.d.	b.d.
Al_2O_3	1.23	1.22	2.86	2.09	1.52	1.35	1.27
Cr_2O_3	b.d.	b.d.	b.d.	b.d.	b.d.	0.08	0.13
Y_2O_3	0.55	0.48	0.88	1.05	1.18	1.66	1.35
La_2O_3	13.58	13.88	14.29	13.68	6.07	6.45	6.56
Ce_2O_3	21.18	20.01	20.72	20.89	16.73	16.78	17.06
Pr_2O_3	1.57	1.40	1.38	1.47	2.15	2.11	2.12
Nd_2O_3	4.24	3.77	3.78	3.87	9.28	8.65	8.90
Sm_2O_3	0.41	0.29	0.37	0.34	1.56	1.50	1.60
Gd_2O_3	0.10	0.14	b.d.	0.12	0.69	0.82	0.71
Tb_2O_3	b.d.	b.d.	b.d.	b.d.	0.09	0.08	0.09
Dy_2O_3	0.13	0.10	0.16	0.19	0.33	0.46	0.40
Er_2O_3	0.05	0.02	0.09	0.09	0.08	0.12	0.09
Yb_2O_3	0.05	0.02	0.08	0.08	0.02	0.03	0.02
MgO	0.25	0.24	0.25	0.24	0.01	0.03	0.02
CaO	3.45	3.97	4.60	3.50	5.66	5.47	5.48
MnO	0.08	0.08	0.08	0.06	0.05	0.08	0.08
FeO*	9.60	9.43	8.27	9.84	7.83	8.89	9.23
PbO	b.d.	b.d.	b.d.	b.d.	b.d.	b.d.	b.d.
P_2O_5	0.11	0.11	0.37	0.14	0.44	0.45	0.40
Nb_2O_5	0.24	0.24	0.45	0.33	1.31	3.05	3.07
Ta_2O_5	b.d.	0.05	b.d.	0.06	0.03	0.08	0.09
WO_3	0.05	0.09	0.12	0.42	0.05	0.04	0.06
TOTAL	98.07	97.85	99.41	98.56	100.37	99.13	99.67

b.d. = below detection limit. FeO* = total Fe calculated as FeO.

Cations based on 22 oxygens

Si	3.998	4.032	4.045	4.131	4.218	3.924	3.938
Ti	2.806	2.823	2.619	2.514	2.838	2.650	2.628
Zr	0.158	0.161	0.216	0.169	0.247	0.272	0.269
Hf	0.004	0.006	0.007	0.009	0.011	0.011	0.013
Th	0.102	0.127	0.000	0.077	0.008	0.012	0.011
U	0.004	0.002	0.001	0.002	0.000	0.000	0.000
Al	0.300	0.296	0.663	0.505	0.339	0.314	0.296
Cr	0.000	0.000	0.000	0.000	0.000	0.013	0.021
Y	0.061	0.052	0.092	0.114	0.119	0.175	0.141
La	1.037	1.054	1.037	1.032	0.424	0.470	0.478
Ce	1.606	1.508	1.493	1.564	1.160	1.215	1.233
Pr	0.118	0.105	0.099	0.110	0.148	0.152	0.152
Nd	0.313	0.277	0.266	0.283	0.628	0.611	0.627
Sm	0.029	0.020	0.025	0.024	0.102	0.102	0.109
Gd	0.007	0.009	0.000	0.008	0.043	0.054	0.047
Tb	0.000	0.000	0.000	0.000	0.006	0.005	0.006
Dy	0.009	0.007	0.010	0.012	0.020	0.029	0.026
Er	0.003	0.001	0.006	0.006	0.005	0.008	0.005
Yb	0.003	0.001	0.005	0.005	0.001	0.002	0.001
Mg	0.077	0.073	0.073	0.074	0.004	0.008	0.007
Ca	0.765	0.875	0.970	0.768	1.148	1.158	1.159
Mn	0.014	0.015	0.014	0.011	0.009	0.014	0.014
Fe	1.663	1.623	1.360	1.683	1.240	1.471	1.524
Pb	0.000	0.000	0.000	0.000	0.000	0.000	0.000
P	0.019	0.019	0.062	0.024	0.071	0.076	0.066
Nb	0.023	0.022	0.040	0.030	0.112	0.273	0.273
Ta	0.000	0.003	0.000	0.003	0.002	0.004	0.005
W	0.001	0.002	0.002	0.007	0.001	0.001	0.001
TOTAL	13.120	13.113	13.105	13.165	12.904	13.024	13.050

Figure captions

FIGURE 1. Map showing the geographical and geological extent of tholeiitic suites containing chevkinite/perrierite in Western Australia. Kimberley, Pilbara and Yilgarn: stable cratons. Halls Creek Orogen (HCO), Gascoyne Province (GP), Pinjarra Orogen (PO) and Albany-Fraser Orogen (AFO): Proterozoic orogenic belts. Numbers refer to descriptions in Table 1.

FIGURE 2. Chevkinite/perrierite in lunar mare basalt 10047 (227). (a) Plane polarized light (PPL) image. (b) Backscattered electron image (BSE) of the same grain showing pocket of mesostasis between plagioclase (pl) and cristobalite (crs), with c/p (chv), baddeleyite (bdy) and native Fe.

FIGURE 3. Chevkinite/perrierite in tholeiitic dolerites. (a) PPL image of prismatic c/p (red-brown) and apatite (pale blue in top left) with quartz and cloudy orthoclase. (b) BSE image of the c/p crystal shown in (a) showing granophyric quartz-orthoclase intergrowth. (c) PPL image of inclusions of ilmenite and c/p in brown igneous hornblende. (d) BSE image of c/p enclosed in hornblende on the margin of clinopyroxene (augite and pigeonite). The oval impression is an ion microprobe analysis spot. (e) Hornblende and ilmenite with small crystal of brown c/p. Note dark halo in hornblende adjacent to c/p. (f) BSE image of the c/p crystal shown in (e). Note faint zoning and mottling at the edge of the crystal. The oval impressions are ion microprobe analysis spots. (a) and (b) Grain 04-13F from dolerite intruding the Manganese Group at Woodie Woodie; (c) from dolerite intruding the Badgeradda Group (not analyzed); (d) Grain 09-09G

620 from dolerite intruding the Eel Creek Formation; (e) and (f) Grain 09-09E from dolerite intruding
621 the Eel Creek Formation. Mineral abbreviations: quartz (qz), plagioclase (pl), ilmenite (ilm),
622 hornblende (hbl), c/p (chv), clinopyroxene (cpx), mesostasis (meso).
623
624 FIGURE 4. Prismatic c/p (Grain 04-121D) in granophyre from the Hart Dolerite. (a) PPL image
625 of color-zoned c/p with zircon (pale blue). (b) BSE image of the same grain showing some
626 zoning and alteration (dark) around grain boundaries and fractures. (c) X-ray distribution map for
627 Ca. Ca is enriched towards grain boundaries and along fractures. (d) X-ray distribution map for
628 Fe. There is an irregular zone of Fe enrichment in the core of the grain. Mineral abbreviation:
629 zircon (zrn).
630
631 FIGURE 5. Elemental plots for c/p from tholeiitic mafic rocks compared with data from other
632 common rock types (shaded fields and open diamond symbols). Analyses from tholeites have
633 more Zr than most rock types, but less than Zr-enriched analyses. (a) Ca + Sr vs Zr (apfu). (b) Ca
634 + Sr + Ti in C-site + Zr vs total REE. Legend in (b) as for (a).
635
636 FIGURE 6. Triangular plot of elements enriched in perrierite (Ca, Sr, Mg, Al) versus those
637 enriched in chevkinite (LREE and Fe). Shaded area is the field of c/p from mafic igneous rocks
638 from Western Australia.
639
640 FIGURE 7. Macdonald and Belkin plots of CaO versus FeO* (wt%). The solid line is the line
641 separating chevkinite from perrierite from Macdonald et al. (2012). (a) Data from all samples:
642 Two groups with >8 wt% FeO* and <8 wt% FeO* are apparent. (b) Data from nine grains (A-G,

I, K) of c/p from Woodie Woodie: High- and low-Fe groups are apparent. Individual grains have almost constant FeO* but variable CaO.

FIGURE 8. TEM images from low-Fe c/p. (a) TEM image showing background phase with multiple nanoparticle inclusions. (b) SAED pattern from the base phase corresponding with the [-111] zone axis of perrierite. (c) TEM elastic image showing nanoinclusions. (d) EFTEM element map for Ti $L_{2,3}$ edge of the area in (c). (e) EFTEM element map for Ce $M_{4,5}$ edge of the area in (c).

FIGURE 9. TEM images from high-Fe c/p. (a) TEM image showing aggregates of fine acicular crystals in amorphous background. (b) SAED pattern from the crystals corresponding with the [001] zone axis of chevkinite. (c) SAED pattern from the amorphous phase.

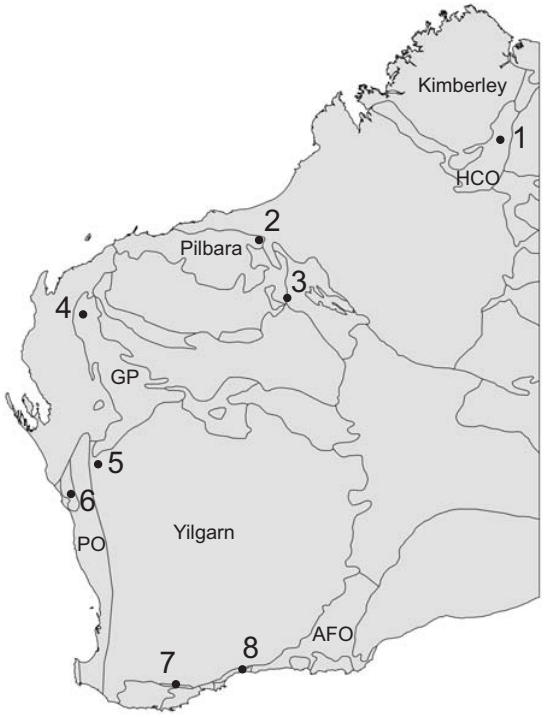

Muhling et al. Fig. 1

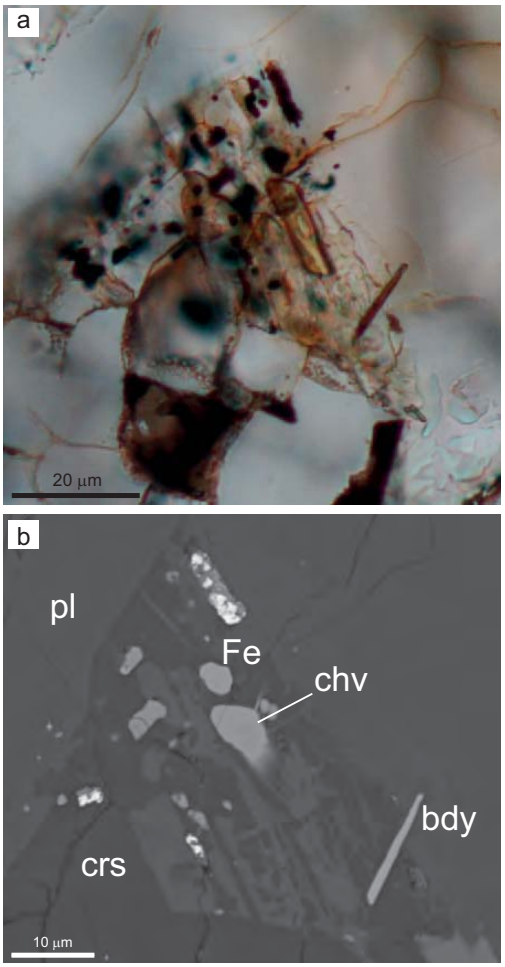

Muhling et al. Figure 2

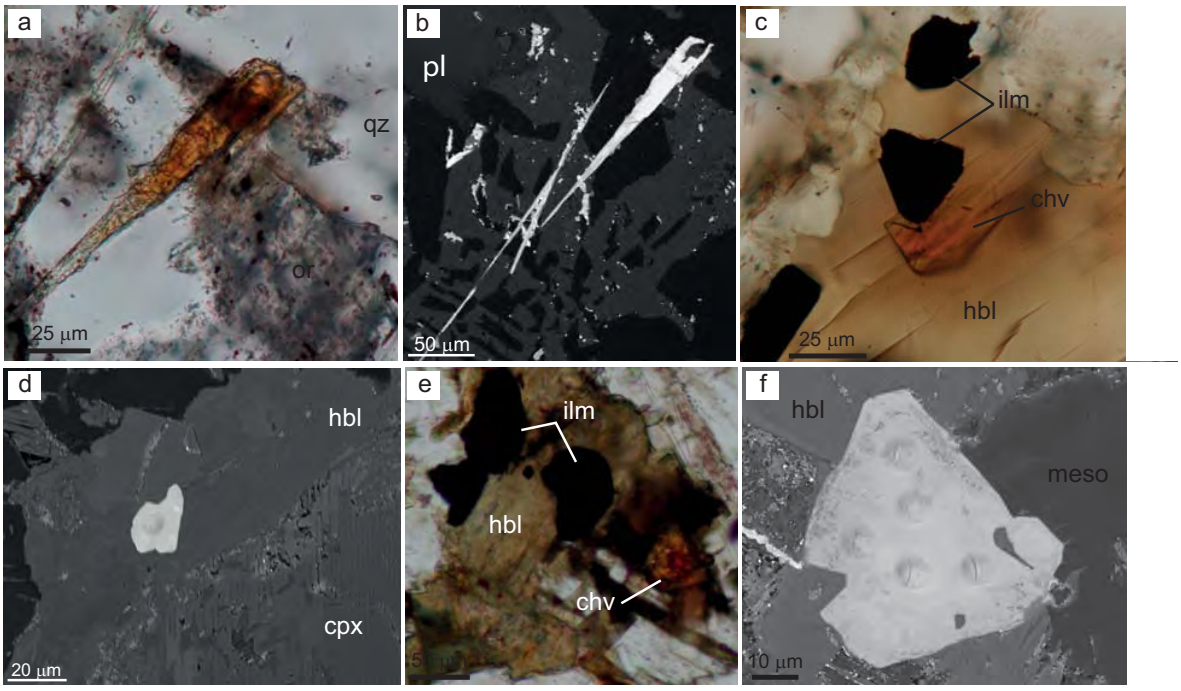

Muhling et al. Fig. 3

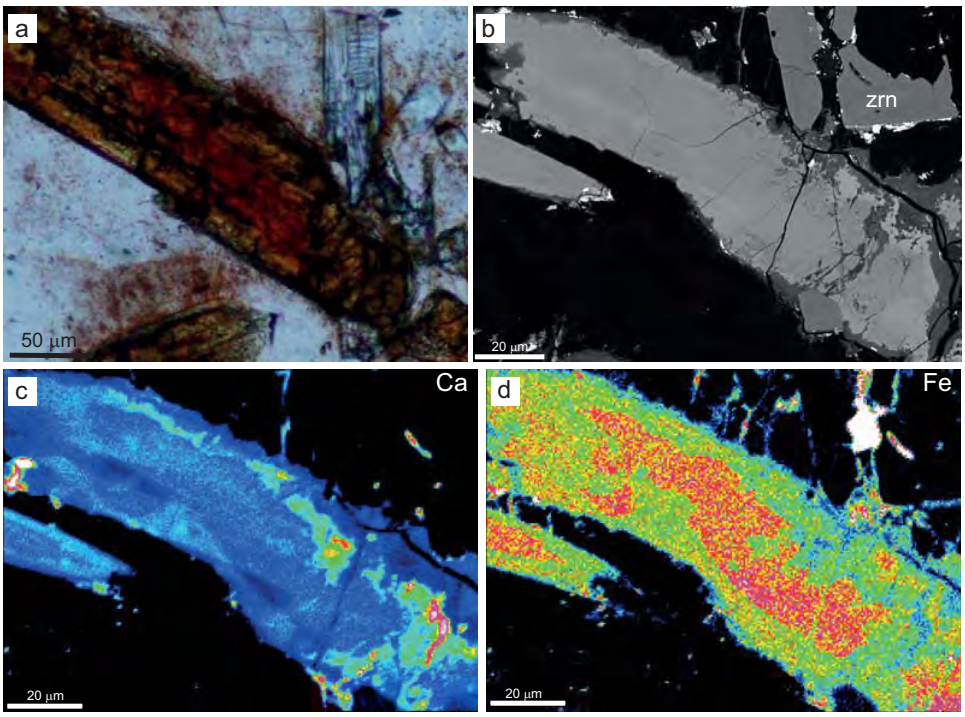

Muhling et al. Fig. 4

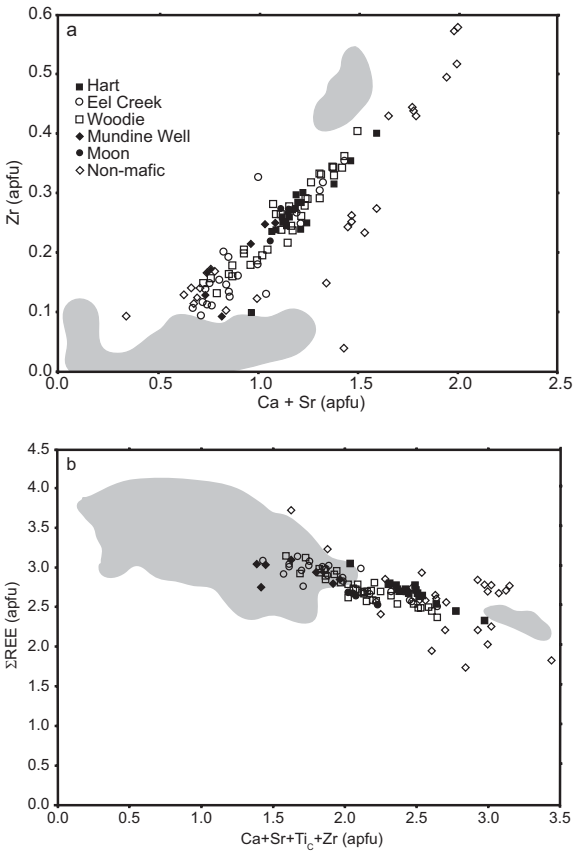

Muhling et al. Fig. 5

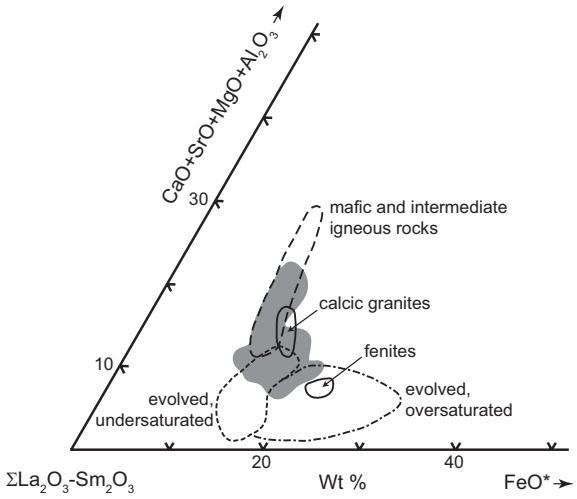

Muhling et al. Fig. 6

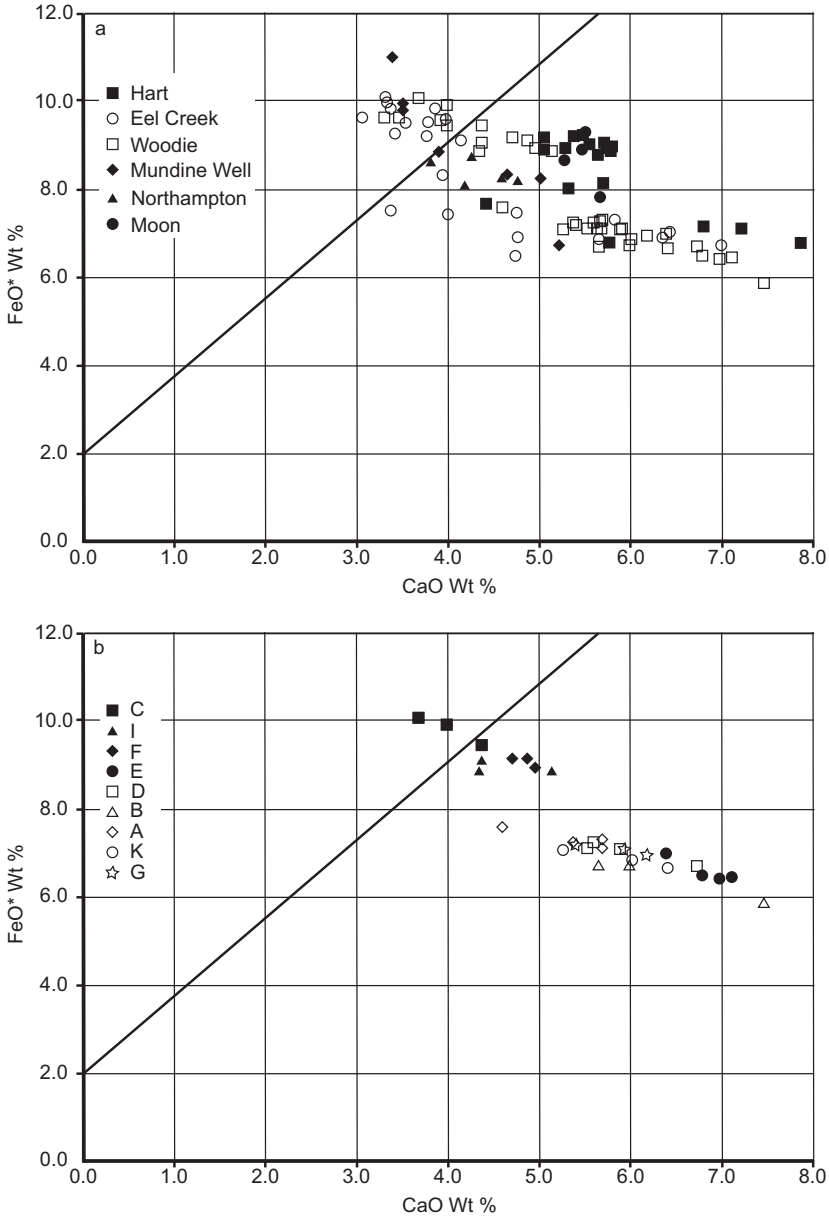

Muhling et al. Fig. 7

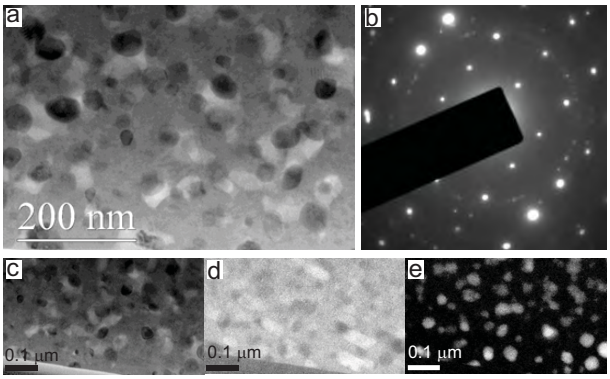

Muhling et al. Figure 8

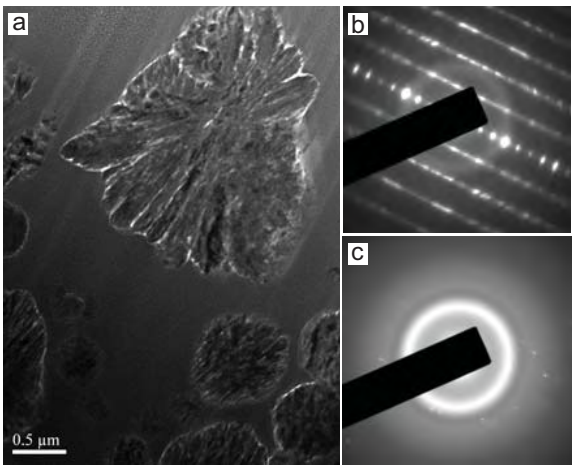

Muhling et al. Fig. 9